scientific reports

Check for updates

OPEN

Observations of the delayed-choice quantum eraser using coherent photons

Sangbae Kim & Byoung S. Ham✉

Quantum superposition is the cornerstone of quantum mechanics, where interference fringes originate in the self-interference of a single photon via indistinguishable photon characteristics. Wheeler's delayed-choice experiments have been extensively studied for the wave-particle duality over the last several decades to understand the complementarity theory of quantum mechanics. The heart of the delayed-choice quantum eraser is in the mutually exclusive quantum feature violating the cause-effect relation. Here, we experimentally demonstrate the quantum eraser using coherent photon pairs by the delayed choice of a polarizer placed out of the interferometer. Coherence solutions of the observed quantum eraser are derived from a typical Mach–Zehnder interferometer, where the violation of the cause-effect relation is due to selective measurements of basis choice.

The delayed-choice experiments proposed by Wheeler in 1978[1] for the complementarity theory[2] have been intensively studied over the last several decades[3–16]. Although the original concept of the complementarity theory is for the exclusive nature between non-commutable entities such as position and momentum, delayed choice experiments have been developed for the measurement control of the wave-particle duality in an interferometric system[3]. The wave-particle duality of a single photon shows a trade-off relation between the wave nature-based fringe visibility and particle nature-based which-way information[4]. The delayed choice experiments have been broadly demonstrated using thermal lights[5], entangled photons[6–8], atoms[9–11], neutrons[3], attenuated lasers[4,12,13], and antibunched single photons[14,15]. In the delayed choice, a post-control of measurements results in a paradoxical phenomenon of violation of the cause-effect relation[16]. The quantum eraser is based on the post-choice of measurements, choosing[17] or erasing[18] one of the natures. Recently, the quantum eraser has been developed for reversing a given nature via post-measurements using entangled photons[19], coherent photons[13,20], thermal lights[21], and antibunched photons[11,22].

In the present paper, the delayed-choice quantum eraser was experimentally demonstrated using coherent photons via polarization basis controls, where the coherent photons are obtained from an attenuated continuous wave (cw) laser. Like some delayed-choice schemes[13,14,18,19,21], the present one is for the post-control of the pre-determined photon nature. Here, our Mach–Zehnder interferometer (MZI) composed of a polarizing beam splitter (PBS) and a beam splitter (BS) is set for the particle nature according to the Fresnel-Arago law[23] or noninteracting quantum operators[24]. Thus, the which-way information of a single photon inside the MZI is a pre-determined fact, resulting in no interference fringes in the output ports of the MZI. Without controlling the MZI itself, however, we experimentally retrieve the wave nature of the photon by controlling the output photon's polarization basis using a polarizer[13,14,19,21]. If the post-measurements show an interference fringe, it represents the violation of the cause-effect relation because the choice of the polarizer satisfies the space-like separation. For this, we measured first- and second-order intensity correlations using a coincidence counting unit.

Experimental setup

Figure 1 shows the schematic of the present delayed-choice quantum eraser using coherent photons generated from an attenuated cw laser (see "Methods" section). For Fig. 1, a coincidence counting unit (CCU, DE2; Altera) is used for both first- and second-order intensity correlations between two detectors D1 and D2 (SPCM-AQRH-15, Excelitas). For the second-order correlation, only doubly bunched photons are counted by CCU, where the generation ratio of doubly-bunched photons to single photons is ~ 1% at the mean photon number $\langle n \rangle \sim 0.01$ (see Sect. A of the Supplemental Materials). For the first-order intensity correlation, both input channels of CCU from D1 and D2 are measured individually for a period of 0.1 s per data point (see Fig. 2). The

Center for Photon Information Processing, and School of Electrical Engineering and Computer Science, Gwangju Institute of Science and Technology, 123 Chumdangwagi-ro, Buk-gu, Gwangju 61005, South Korea. ✉email: bham@gist.ac.kr

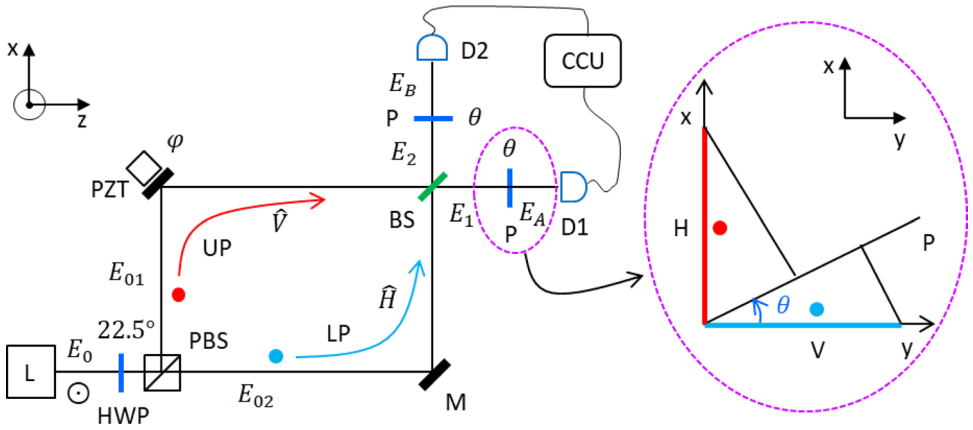

Figure 1. Schematic of the quantum eraser. (Dotted circle) Projection onto a polarizer. L: laser, HWP: half-wave plate, PBS: polarizing beam splitter, H (V): horizontal (vertical) polarization, M: mirror, PZT: piezo-electric transducer, BS: beam splitter, P: polarizer, D1/D2: single photon detector. CCU: coincidence counting unit. The light of laser L is vertically polarized with respect to the plane of incidence. Each colored dot indicates a single photon having the same probability amplitude.

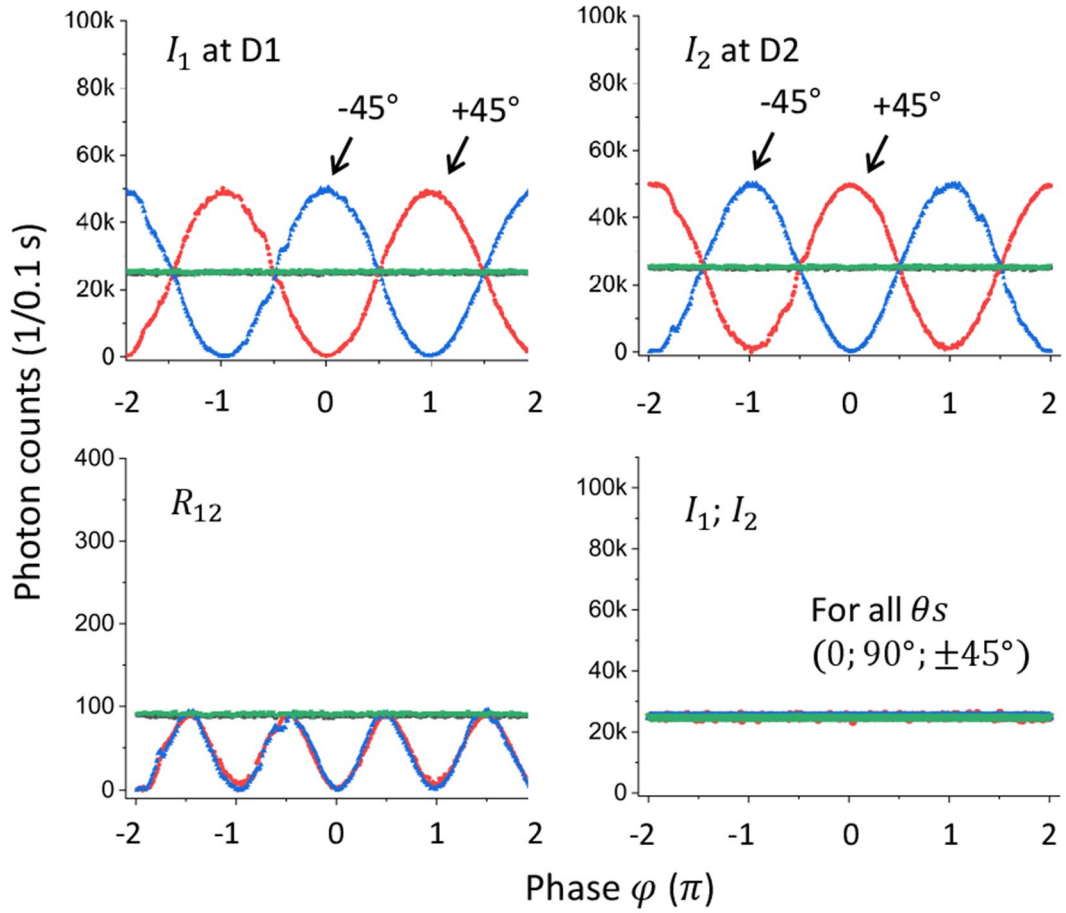

Figure 2. Experimental observations of the delayed-choice quantum eraser. (upper panels) Red: $\theta = 45°$, Blue: $\theta = -45°$, Green: $\theta = 0°$, Black: $\theta = 90°$. $\Delta L \ll l_c$, where ΔL is the path-length difference between UP and LP. l_c is the coherence length of the laser L. (lower left panel) Coincidence detection for the upper panels (color matched). (lower right panel) $\Delta L \gg l_c$ for upper panels ($\theta = \pm 45°; 0°; 90°$). Photon counts are for 0.1 s. The total data points for each θ in each panel are 360. The measured statistical error in each data is less than 1% (see Supplementary Materials).

higher-order bunched photons are neglected by Poisson statistics (see Sect. A of the Supplemental Materials). To provide polarization randomness of a single photon, a 22.5°-rotated half-wave plate (HWP) is placed just before the MZI. By the following PBS, the single photon inside the MZI shows distinguishable photon characteristics with perfect which-way information: $|\psi\rangle_{MZI} = \frac{1}{\sqrt{2}}(|V\rangle_{UP} + |H\rangle_{LP})$. Thus, the measured photons outside the MZI show the predetermined particle nature of a single photon (not shown), as in refs.[13,14,19].

Due to the predetermined distinguishable photon characteristics of the particle nature, the MZI does not result in a φ-dependent interference fringe for the output photons (E_1; E_2). As demonstrated[14,19], this is due to noninterfering quantum operators[24] or simply by the Fresnel-Arago law[23]. Due to the classical physics of the cause-effect relation, the action of polarizers (Ps) outside the MZI for the output photons (E_1; E_2) should not change the predetermined photon nature inside the MZI. To satisfy the space-like separation, the length of each arm of the MZI is set to be 2 m, corresponding > 6ns in the delayed choice of P. Regarding the temporal resolution (< 1ns) of the single photon detector as well as the CCU (6 ns), the condition of the space-like separation is satisfied. Thus, any violating measurements should belong to the quantum mystery of the delayed-choice quantum eraser.

The polarizer's rotation angle θ is with respect to the vertical axis $\hat{y}$, as shown in the Inset. E_0 denotes an amplitude of a single photon. The mean photon number is set at $\langle n\rangle \sim 0.01$ to satisfy incoherent and independent conditions of statistical measurements, resulting in the mean photon-to-photon separation (600 m) far greater than the coherence length (3 mm) of the cw laser (see Sect. A of the Supplemental Materials). Doubly-bunched photon pairs are also satisfied for this condition. Thus, the measurements of Fig. 1 are for a statistical ensemble of single photons controlled by Ps.

For the MZI phase control φ, the path-length difference (ΔL) is adjusted to be far less than the coherence length l_c (3 mm). This MZI coherence condition is easily tested for the same polarization-based MZI interference. Thus, the MZI in Fig. 1 satisfies a general scheme of single-photon (noninterfering) interferometers[25]. Each output photon (E_1 or E_2) from the MZI can be represented by a superposition state of the orthonormal polarization bases at equal probability amplitudes: $|\psi\rangle_{out} = \frac{1}{\sqrt{2}}\left(|V\rangle e^{i\varphi} + |H\rangle\right)$. This polarization-basis randomness of the MZI output photons originates in the random polarization bases provided by the 22.5°-rotated HWP. In ref.[14], the measurement control with Ps in Fig. 1 is replaced by a linear optics-combined electro-optic modulator (EOM) system. By this EOM switching module, the same MZI scheme as in Fig. 1 is satisfied for the post-control of output photons[14]. Classical photon cases have also been discussed for the same results of the quantum eraser[20,21], where different analyses have been separately presented[5,11,22].

Analysis

To coherently interpret the delayed-choice quantum eraser in Fig. 1, the PBS-BS MZI is analyzed using a coherence approach:

$$\begin{bmatrix} E_1 \\ E_2 \end{bmatrix} = \frac{E_0}{\sqrt{2}}[BS][\Phi]\begin{bmatrix} E_{01} \\ E_{02} \end{bmatrix} = \frac{E_0}{2}\begin{bmatrix} i(\hat{H} + \hat{V}e^{i\varphi}) \\ \hat{H} - \hat{V}e^{i\varphi} \end{bmatrix}, \tag{1}$$

where $[BS] = \frac{1}{\sqrt{2}}\begin{bmatrix} 1 & i \\ i & 1 \end{bmatrix}$ and $[\Phi] = \begin{bmatrix} 1 & 0 \\ 0 & e^{i\varphi} \end{bmatrix}$[26]. E_0 is the amplitude of a single photon. $\widehat{V}$ ($\widehat{H}$) represents a unit vector of the vertical (horizontal) polarization component of the input photon E_0: $|V\rangle = \widehat{V}E_0$ and $|H\rangle = \widehat{H}E_0$. The inputs of E_1 and E_2 by the 22.5°-rotated HWP and PBW are analyzed in Sect. D of Supplementary Material using Mueller matrix: $\boldsymbol{E}_{01} = i\widehat{V}\frac{E_0}{\sqrt{2}}$; $\boldsymbol{E}_{02} = \widehat{H}\frac{E_0}{\sqrt{2}}$. The role of the 22.5°-rotated HWP is to give an equal probability amplitude of orthogonally polarized photons to PBS. Here, the 4 × 1 matrix of path-polarization tensor products reduces down to a 2 × 1 matrix by PBS, resulting in the vertical (horizontal) polarization-upper (lower) path correlation. The coherence approach of Eq. (1) is for the wave nature of a photon, resulting in no photon number dependent. Instead, phase information is critical[13,20,21]. Most importantly, interference between the $\widehat{H}$- and $\widehat{V}$-polarizations of a photon on the BS shows independent photon characteristics in both output ports (E_1; E_2) due to noninteracting orthogonal polarization bases[23,24]. Thus, the calculated mean intensities of E_1 and E_2 in Eq. (1) are $\langle I_1\rangle = \langle I_2\rangle = \langle I_0\rangle/2$, regardless of φ, where $I_0 = E_0E_0^*$. These are the coherence solutions of the PBS-BS MZI for the particle nature of a single photon with perfect which-way information, resulting in distinguishable photon characteristics.

By inserting a polarizer (P) outside the MZI, Eq. (1) is coherently rewritten for the polarization projection on P (see Inset of Fig. 1):

$$\boldsymbol{E_A} = \frac{iE_0}{2}\left(sin\theta + cos\theta e^{i\varphi}\right)\widehat{p}, \tag{2}$$

$$\boldsymbol{E_B} = \frac{E_0}{2}\left(sin\theta - cos\theta e^{i\varphi}\right)\widehat{p}, \tag{3}$$

where θ is the rotation angle of P. Thus, Eqs. (2) and (3) represent polarization projections of the output photon onto the polarizers: $\widehat{V} \rightarrow \widehat{p}cos\theta$ and $\widehat{H} \rightarrow \widehat{p}sin\theta$. Here, the positive θ is for the clockwise direction from the vertical axis of the photon propagation direction (z) (see the Inset of Fig. 1). For the negative rotation, however, the projections are denoted by $\widehat{V} \rightarrow \widehat{p}cos\theta$ and $\widehat{H} \rightarrow -\widehat{p}sin\theta$. The projection onto the polarizer P represents the action of the delayed choice for the quantum eraser.

The calculated mean intensities of Eqs. (2) and (3) are as follows:

$$\langle I_A \rangle = \frac{\langle I_0 \rangle}{4} \langle 1 + sin2\theta cos\varphi \rangle, \tag{4}$$

$$\langle I_B \rangle = \frac{\langle I_0 \rangle}{4} \langle 1 - sin2\theta cos\varphi \rangle, \tag{5}$$

Equations (4) and (5) are the analytical solutions of the quantum eraser in Fig. 1 (see also Fig. 2). Here, the MZI coherence is for every single photon, resulting in the self-interference in the MZI[25]. Due to the low mean photon number, no coherence exists between consecutive photons, satisfying the condition of a statistical ensemble. For $\theta = 0$, the original distinguishable photon characteristics appear with no interference fringes regardless of φ.

For $\theta = \pm\frac{\pi}{4}(\pm 45°)$, Eqs. (4) and (5) are rewritten for the first-order intensity correlation:

$$\langle I_A \rangle = \frac{\langle I_0 \rangle}{4} \langle 1 \pm cos\varphi \rangle, \tag{6}$$

$$\langle I_B \rangle = \frac{\langle I_0 \rangle}{4} \langle 1 \mp cos\varphi \rangle. \tag{7}$$

For Eqs. (6) and (7), the same P-projected photon measurements have been demonstrated in refs.[14,15] for single photons and a polarizer in ref.[19], resulting in the quantum eraser using entangled photons. Although the EOM block control looks like a direct control of the MZI[14], it corresponds to the combination of PBS and P in Fig. 1 (see Sect. B of the Supplemental Materials). In SPDC processes, entangled photons automatically satisfy both $\pm$ signs in Eqs. (6) and (7) via spatial mixing of the signal and idler photons[27]. This is the fundamental difference between coherent photons and entangled photon pairs for the quantum eraser[28]. The sum of the polarization bases in Eqs. (6) and (7), thus, corresponds to the entangled photon-pair case, as long as it deals with the first-order intensity correlation[19]. Regarding the causality violation, thus, Eqs. (6) and (7) witness the quantum feature of the delayed-choice quantum eraser for Fig. 1. Total intensity through Ps is uniform at 50% photon loss regardless of the angle of the polarizers. This selective measurement by P at the cost of 50% event loss is the origin of the quantum eraser, as differently argued for no choice of quantum eraser[29].

The second-order intensity correlation R_{AB} via coincidence detection between D1 and D2 in Fig. 1 shows the intensity product between Eqs. (6) and (7):

$$R_{AB} = \frac{I_0^2}{4}(1 - cos2\varphi), \tag{8}$$

where a doubly-bunched photon pair relates to $2I_0$. Compared with ref.[19] based on entangled photons, the doubled oscillation in Eq. (8) is due to the out-of-phase fringes in D1 and D2, resulting in a classical nature. Unlike coincidence detection-caused nonlocal correlation, Eq. (8) is not for the quantum feature of a joint-phase relation[28]. This is because there is no such joint-phase action by polarizers (discussed elsewhere)[30].

Experimental results

The upper panels of Fig. 2 show the experimental proofs of the delayed-choice quantum eraser in Fig. 1 for coherent single photons measured by D1 and D2, respectively, for two different θs. As expected from Eqs. (6) and (7), fringes appear in both measurements for $\theta = \pm 45°$. However, no fringe appears for $\theta = 0°; 90°$, as expected by Eqs. (4) and (5) (see the overlapped green and black lines). The observed fringes represent the wave nature of the photon inside the MZI in Fig. 1. The statistical error (standard deviation) in single photon measurements is less than 1% (see Sect. A of Supplemental Materials). This is a big benefit of using coherent photons from a stabilized laser compared to entangled photons from spontaneous parametric down-conversion process (SPDC) or anti-bunched photons from N-V color centers, whose respective photon counts are less than 10%[19] and 1%[14] of Fig. 2. Because the PB-MZI is not actively stabilized, most errors are from the air turbulence affecting MZI path lengths. Under normal lab conditions, the PB-MZI is stabilized for as long as a few minutes, where the total data collection time of each panel in Fig. 2 is 36 s (see Sect. C of Supplementary Materials).

The lower left panel of Fig. 2 is for coincidence detection for the upper panels (color matched). The photon counts for the coincidence detection in the lower left panel are less than 1% of those in the upper left panel of single photons. This is due to Poisson statistics for $\langle n \rangle \sim 0.01$. As expected in Eq. (8) for the coherence product, the doubled fringe oscillation period is the direct result of the intensity product between them showing the classical nature. This intensity product of the lower left panel has nothing to do with the nonlocal quantum feature due to different purposes without independent local control parameters[19,30].

The lower right panel of Fig. 2 is for the incoherence condition of each photon by setting the MZI path-length difference (ΔL) far greater than the coherence length l_c of the laser. As shown, the single photon's coherence in the MZI is the key to the quantum eraser. This fact has never been discussed seriously so far, even though it seems to be obvious[16]. The observed fringes in Fig. 2 for the first-order intensity correlation demonstrate the same mysterious quantum eraser[14] because the predetermined particle nature of the photon inside the MZI (see the green line) cannot be controlled or changed by the post-measurements of the output photons[13,14,19]. Due to the benefit of coherence optics, the observed visibilities in the upper panels of Fig. 2 are near perfect.

Conclusion

The delayed-choice experiments were conducted for the quantum eraser via post-control of polarization basis of coherent photons in a coincidence detection scheme for the first-order intensity correlation. Corresponding coherence solutions were also derived in the same setups for the quantum eraser. Like conventional delayed-choice quantum erasers using orthogonal polarization bases, predetermined photon characteristics of the particle nature were retrospectively converted into the wave nature via post-selected polarization-basis projection, resulting in the violation of the cause-effect in classical physics, where the predetermined which-way information of photons was completely erased by the post-choice of the polarizer satisfying the space-like separation. The cost of the post-measurements by the polarizer is a 50% loss of measurement events. As usual in nonlocal quantum features, the observed quantum eraser was also due to the selective measurements of the mixed polarization bases.

Methods

In Fig. 1, the laser L is SDL-532-500 T (Shanghai Dream Laser), whose center wavelength and coherence length are 532 nm and 3 mm, respectively. The laser light is vertically polarized. For the random but orthogonal polarizations of a single photon, a half-wave plate (HWP) is rotated by 22.5 degrees from its fast axis. For a single photon, the laser L is attenuated by neutral density filters, satisfying Poisson distribution (see Supplementary Materials). The measurements for both output photons from the MZI are conducted by CCU (DE2; Altera) via a set of single photon detectors D1 and D2 (SPCM-AQRH-15, Excelitas). The dead time and dark count rate of the single photon detectors are 22 ns and 50 counts/s, respectively. The resolving time of the single photon detector is ~ 350 ps, whose converted electrical pulse duration is ~ 6 ns. For the polarization projection by Ps in Fig. 1, four different rotation angles are set (− 45, 0, 45, or 90 degrees) to the clockwise direction with respect to the vertical axis of the light propagation direction. The photon counts for each data point in Fig. 2 are measured by CCU for 0.1 s and calculated by a homemade Labview program.

In Fig. 2, the mean photon number is set at $\langle n \rangle \sim 0.01$. The maximum number of measured single photons in each MZI output port is ~ a half million per second, resulting in the mean photon-to-photon distance of 600 m. Compared with the laser's coherence length of 3 mm, it is clear that the measured single photons are completely independent and incoherent among them. On behalf of the polarizing beam splitter (PBS), perpendicularly and horizontally polarized components of an incident photon are separated into the upper (UP) and lower paths (LP), respectively. Both split components of a single photon are recombined in the BS, resulting in PB (PBS-BS)-MZI. Thus, the photons in the PB-MZI in Fig. 1 behave as the particle nature, resulting in no interference fringes in the output ports. In other words, the photons inside the MZI represent perfect which-way information or distinguishable characteristics.

The length of each arm of the PB-MZI is set at 2 m, and the path-length difference between UP and LP is kept to be far less than 3 mm to satisfy the coherence condition of each photon. This coherence condition is essential for delayed-choice quantum eraser experiments. The φ phase control of the PB-MZI is conducted by a piezo-electric optic mount (PZT; KC1-PZ, Thorlabs) connected by a PZT controller (MDT693A, Thorlabs) and a function generator (AFG3021, Tektronix). For Fig. 2, the data is measured under the φ scanning mode, where the phase resolution is $\frac{2\pi}{180}$ radians. Thus, Fig. 2 has 180 data points for a 2 π cycle of φ (see Table S1 of the Supplementary materials). The BS position for the recombination of two split components of a single photon is well-adjusted for a complete overlap between them.

Data availability

All data generated or analyzed during this study are included in this published article.

Received: 8 March 2023; Accepted: 6 June 2023
Published online: 16 June 2023

References

1. Wheeler, J. A. In *Mathematical Foundations of Quantum Theory*, Marlow, A. R. Ed. (Academic Press, 1978), pp. 9–48.
2. Bohr, N. In *Quantum Theory and Measurement*, J.A. Wheeler, W.H. Zurek, Eds. (Princeton Univ. Press, Princeton, NJ, 1983), pp. 9–49.
3. Scully, M. O., Englert, B.-G. & Walther, H. Quantum optical tests of complementarity. *Nature* **351**, 111–116 (1991).
4. Schwindt, P. D. D., Kwiat, P. G. & Englert, B.-G. Quantitative wave-particle duality and nonerasing quantum eraser. *Phys. Rev. A* **60**, 4285–4290 (1999).
5. Peng, T., Chen, H., Shih, Y. & Scully, M. O. Delayed-choice quantum eraser with thermal light. *Phys. Rev. Lett.* **112**, 180401 (2014).
6. Garg, A. & Mermin, N. D. Detector inefficiencies in the Einstein-Podolsky-Rosen experiment. *Phys. Rev. D* **35**, 3831–3835 (1987).
7. DuÈrr, S., Nonn, T. & Rempe, G. Origin of quantum-mechanical complementarity probed by a `which-way' experiment in an atom interferometer. *Nature* **395**, 33–37 (1998).
8. Ionicioiu, R., Jennewein, T., Mann, R. B. & Terno, D. R. Is wave-particle objectivity compatible with determinism and locality?. *Nat. Commun.* **5**, 4997 (2014).
9. Wang, K., Xu, Q., Zhu, S. & Ma, X.-S. Quantum wave-particle superposition in a delayed-choice experiment". *Nat. Photon.* **13**, 872–877 (2019).
10. Manning, A. G., Khakimov, R. I., Dall, R. G. & Truscott, A. G. Wheeler's delayed-choice gedanken experiment with a single atom. *Nat. Phys.* **11**, 539–542 (2015).
11. Aharonov, Y. & Zubairy, M. S. Time and the quantum: erasing the past and impacting the future. *Science* **307**, 875–879 (2005).
12. Ionicioiu, R. & Terno, D. R. Proposal for a quantum delayed-choice experiment. *Phys. Rev. Lett.* **107**, 230406 (2011).
13. Dimitrova, T. L. & Weis, A. Single photon quantum erasing: a demonstration experiment. *Eur. J. Phys.* **31**, 625 (2010).
14. Jacques, V. *et al.* Experimental realization of wheeler's delayed-choice Gedanken experiment. *Science* **315**, 966–978 (2007).
15. Tang, J.-S. *et al.* Realization of quantum Wheeler's delayed-choice experiment. *Nat. Photon.* **6**, 600–604 (2002).
16. Ma, X.-S., Kofler, J. & Zeilinger, A. Delayed-choice gedanken experiments and their realizations". *Rev. Mod. Phys.* **88**, 015005 (2016).

17. Scully, M. O. & Drühl, K. Quantum eraser: A proposed photon correlation experiment concerning observation and "delayed choice" in quantum mechanics. *Phys. Rev. A* **25**, 2208–2213 (1982).
18. Kim, Y.-H., Yu, R., Kulik, S. P. & Shih, Y. Delayed, "choice" quantum eraser. *Phys. Rev. Lett.* **84**, 1–5 (2000).
19. Herzog, T. J., Kwiat, P. G., Weinfurter, H. & Zeilinger, A. Complementarity and the quantum eraser. *Phys. Rev. Lett.* **75**, 3034–3037 (1995).
20. Chur, B. R. & Yudichak, T. W. Classical model of a delayed-choice quantum eraser. *Phys. Rev. A* **103**, 062213 (2021).
21. Dou, L.-Y., Silberberg, Y. & Song, X.-B. Demonstration of complementarity between path information and interference with thermal light. *Phys. Rev. A* **99**, 013825 (2019).
22. Kastner, R. E. The 'delayed choice quantum eraser' neither erases nor delays. *Found. Phys.* **49**, 717–727 (2019).
23. Henry, M. Fresnel-Arago laws for interference in polarized light: A demonstration experiment". *Am. J. Phys.* **49**, 690–691 (1981).
24. Hardy, L. Source of photons with correlated polarizations and correlated directions. *Phys. Lett. A* **161**, 326–328 (1992).
25. Grangier, P., Roger, G. & Aspect, A. Experimental evidence for a photon anticorrelation effect on a beam splitter: A new light on single-photon interferences. *Europhys. Lett.* **1**, 173–179 (1986).
26. Degiorgio, V. Phase shift between the transmitted and the reflected optical fields of a semireflecting lossless mirror is π/2. *Am. J. Phys.* **48**, 81–82 (1980).
27. Zhang, C., Huang, Y.-F., Liu, B.-H., Li, C.-F. & Guo, G.-C. Spontaneous parametric down-conversion sources for multiphoton experiments. *Adv. Quantum Tech.* **4**, 2000132 (2021).
28. Kim, T., Fiorentino, M. & Wong, F. N. C. Phase-stable source of polarization-entangled photons using a polarization Sagnec interferometer". *Phys. Rev. A* **73**, 012316 (2006).
29. Qureshi, T. The delayed-choice quantum eraser leaves no choice. *Intl. J. Theor. Phys.* **60**, 3076–3086 (2021).
30. Ham, B. S. Coherence interpretation of nonlocal quantum correlation in a delayed-choice quantum eraser. arXiv:2206.05358v5 (2022).

Author contributions

S.K. conceived the idea, conducted experiments, and provided the data. B.S.H. developed the idea, analyzed the data, and wrote the manuscript.

Funding

This research was supported by the MSIT (Ministry of Science and ICT), Korea, under the ITRC (Information Technology Research Center) support program (IITP-2023–2021-0–01810) supervised by the IITP (Institute for Information & Communications Technology Planning & Evaluation). BSH also acknowledges that this work was also supported by GIST-GRI 2023.

Competing interests

The authors declare no competing interests.

Additional information

Supplementary Information The online version contains supplementary material available at https://doi.org/10.1038/s41598-023-36590-7.

Correspondence and requests for materials should be addressed to B.S.H.

Reprints and permissions information is available at www.nature.com/reprints.

Publisher's note Springer Nature remains neutral with regard to jurisdictional claims in published maps and institutional affiliations.